

James Webb Space Telescope Initial Mid-Course Correction Monte Carlo Implementation using Task Parallelism

Jeremy Petersen⁽¹⁾, Jason Tichy⁽²⁾, Geoffrey Wawrzyniak⁽³⁾, and Karen Richon⁽⁴⁾
^(1,2,3)*a.i. solutions, Inc., 10001 Dereewood Lane, Lanham, MD 20706, 301-306-1756,*
first.last@ai-solutions.com.

⁽⁴⁾*Code 595.0, NASA Goddard Space Flight Center, 8800 Greenbelt Road, Greenbelt MD,*
20771. 301-286-8845, karen.v.richon@nasa.gov.

The James Webb Space Telescope will be launched into a highly elliptical orbit that does not possess sufficient energy to achieve a proper Sun-Earth/Moon L2 libration point orbit. Three mid-course correction (MCC) maneuvers are planned to rectify the energy deficit: MCC-1a, MCC-1b, and MCC-2. To validate the propellant budget and trajectory design methods, a set of Monte Carlo analyses that incorporate MCC maneuver modeling and execution are employed. The first analysis focuses on the effects of launch vehicle injection errors on the magnitude of MCC-1a. The second on the spread of potential ΔV based on the performance of the propulsion system as applied to all three MCC maneuvers. The final highlights the slight, but notable, contribution of the attitude thrusters during each MCC maneuver. Given the possible variations in these three scenarios, the trajectory design methods are determined to be robust to errors in the modeling of the flight system.

Keywords: *James Webb Space Telescope, Task Parallelism, Monte Carlo, Mid-Course Correction, Libration Point Orbit*

1. Introduction

The James Webb Space Telescope (JWST) is the scientific successor of the Hubble Space Telescope and the Spitzer Space Telescope. Scientific objectives for JWST include identifying the first luminous sources to form and determining the ionization history of the early universe, investigating the assembly of galaxies and the birth of stars and proto-planetary systems, and determining the physical and chemical properties of planetary systems. The science phase of the mission is expected to last 10.5 years. Because of the sensitivity to electromagnetic and thermal radiation involved with observations of these types, JWST will be placed in orbit about the Sun-Earth/Moon L2 libration point (1.5e6 km from Earth), and its optical telescope element (OTE) will be pointed away from the Earth and the Sun. A large sun shield, part of the spacecraft bus element, will block stray light from terrestrial, lunar, and solar radio and light sources. The final element is the integrated science instrument module (ISIM), which houses the cameras and science instruments of the observatory. These three elements comprise the observatory, which appears in Fig. 1.

The observatory will be launched in late 2018 into a highly elliptical orbit that does not possess sufficient energy to achieve an orbit about the Sun-Earth/Moon L2 libration point. Three mid-course correction (MCC) maneuvers will be performed en route to the libration point orbit (LPO) to make up this deficit. A sample trajectory option in the rotating libration point (RLP) frame for the lifetime of the mission appears in Fig. 2 (The RLP frame is attached to the Sun and the Earth, and is centered on the Earth). Naturally, propellant is necessary for these mid-course

correction maneuvers as well as for on-orbit station keeping. At present, propellant-budget analyses are separated into the transfer and the science phases of the mission. The transfer phase is the focus of this investigation. A Monte Carlo analysis that incorporates finite MCC maneuver modeling and execution is employed to validate the propellant budget. These types of analyses are often computationally expensive, but modern computing and parallel processing offer a solution to the computation-cost problem.

This paper is organized as follows: A summary of the JWST mission and the trajectory design with an emphasis on the design algorithm, known as the box method, used for the MCC maneuver design is presented first. The next section focuses on the description of the current propulsion modeling capabilities and the associated statistical variations that are currently modeled. Task parallelism as applied to the JWST MCC Monte Carlo analysis is discussed in the subsequent section. The final section covers three particular analyses that highlight initial results and design implications from MCC Monte Carlo simulations: launch vehicle injection errors, propulsion performance modeling, and effects from the attitude thrusters. Finally, conclusions and future work are discussed.

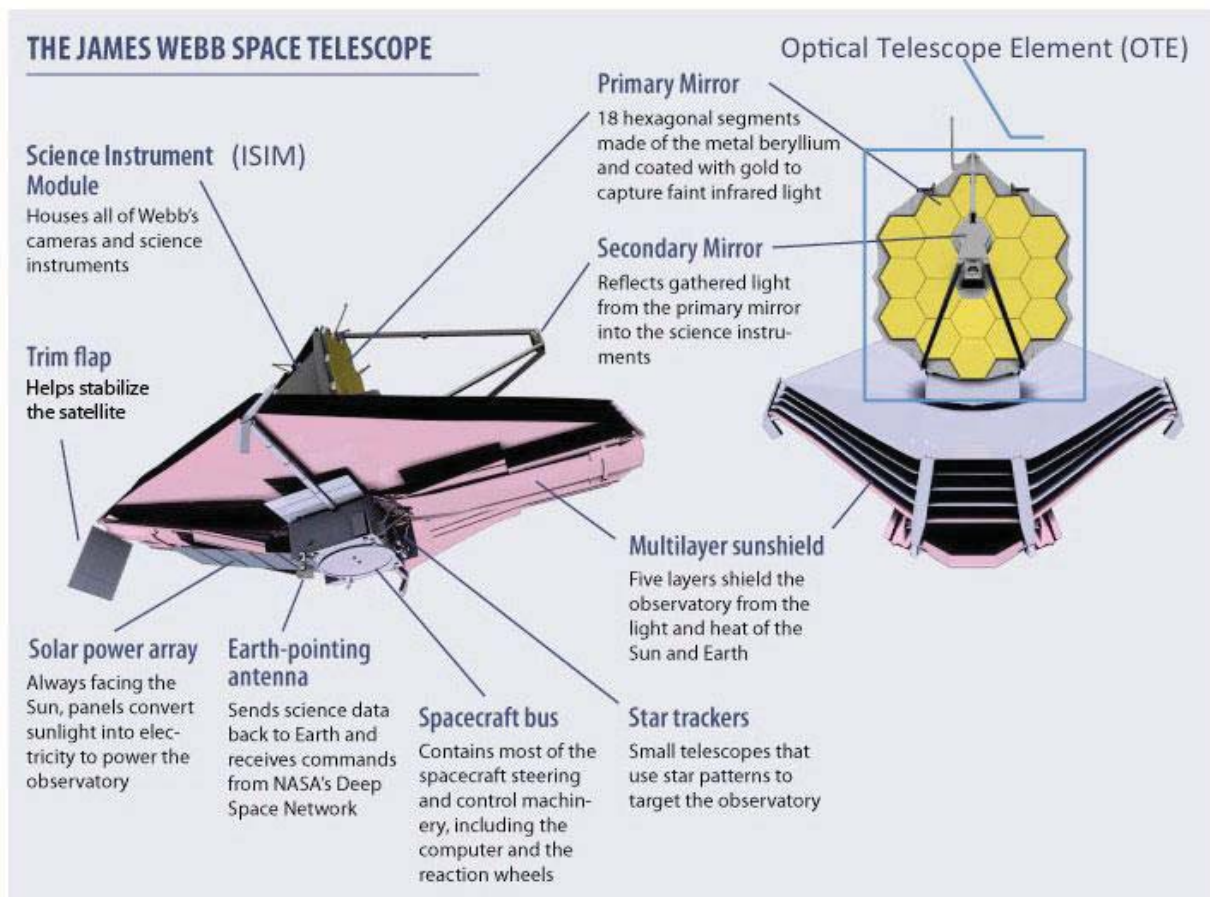


Figure 1. Overview of the JWST Observatory (Image credit: jwst.nasa.gov).

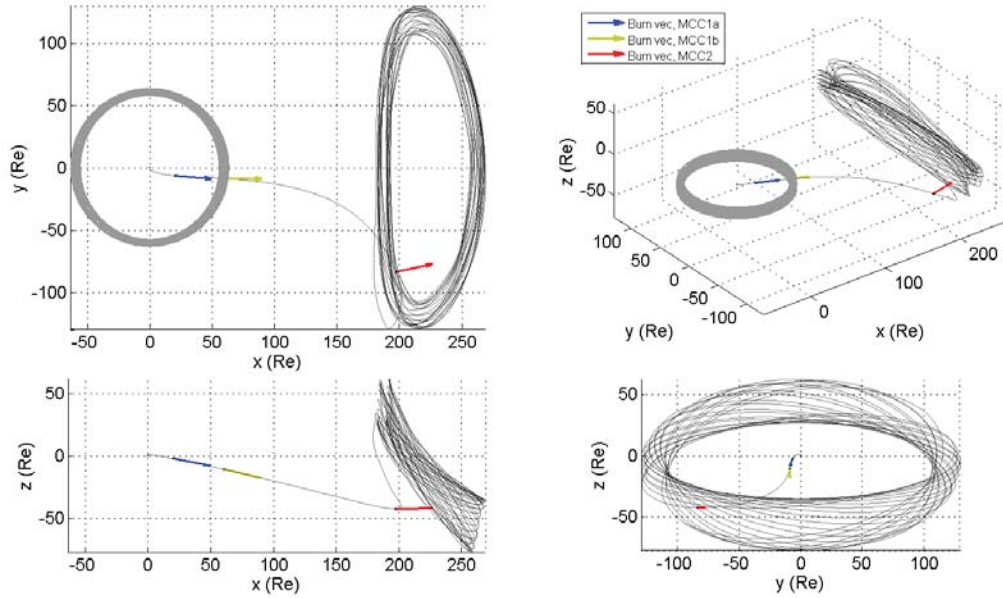


Figure 2. A sample trajectory for the JWST observatory in the RLP frame (the Sun is located along the $-x$ axis). The orbit of the Moon appears for scale in the top two plots. L2 is approximately 235 Earth radii (Re) from the Earth.

2. Trajectory Design Techniques and Challenges

As mentioned, the JWST observatory will be launched into a highly elliptical orbit by an Ariane 5 launch vehicle, requiring three MCC maneuvers to achieve the LPO. The first, MCC-1a, is expected to be a long, continuous burn (potentially up to 3 hours) performed approximately twelve hours after launch. The concept for this maneuver is to execute 95% of the nominal maneuver that would take the observatory directly into the LPO. The decision to execute 95% of the designed maneuver is based on the restriction that the observatory is only capable of adding energy into the trajectory because of attitude constraints. Therefore, this 5% hold-back accounts for unmodeled errors in the execution of the maneuver. If MCC-1a burned “hot,” or added too much energy, the observatory would enter an unrecoverable state beyond the LPO and be lost in deep space. The second maneuver, MCC-1b, is a shorter burn performed approximately 2.5 days after launch that notionally makes up the 5% difference from MCC-1a.¹ The final maneuver, MCC-2, performed 30 days after launch, is designed to correct for any statistical errors remaining in the trajectory prior to entering the LPO.²

Propellant mass is the physical metric that determines the amount of energy available to modify the orbit. The flight dynamics team requires the observatory to achieve a specific ΔV in order to

¹ The duration of MCC-1b will be longer than the 5% reduction in MCC-1a because of the Oberth effect. The observatory has less kinetic energy at MCC-1b compared to MCC-1a. The propulsion system generates less useful energy at lower speeds.

² The final MCC maneuver, MCC-2, could be considered the first station keeping maneuver.

provide the additional energy necessary to achieve an operational LPO. MCC maneuvers are modeled as finite maneuvers; each maneuver has a finite-burn duration and a resulting ΔV . The maneuver duration acts as a proxy for the propellant used in a maneuver. The modeling of the propulsion system determines how much propellant is required to achieve the necessary ΔV . Currently, the cumulative ΔV budget for MCC maneuver is set at 66.5 m/s. The breakdown of the ΔV allocation is as follows: 41 m/s is allocated for MCC-1a, 8 m/s is allocated to compensate for a late MCC-1a (beyond launch plus twelve hours), 7.5 m/s is allocated for MCC-1b, 5 m/s is allocated for MCC-2, and an additional 5 is allocated to add margin for any future design changes.

Modeling the trajectory and associated maneuvers in the simulation begins with the launch vehicle injection state, selecting the launch epoch, and propagating the observatory's trajectory from the resulting state in inertial space to the MCC-1a epoch (launch + 12 hours). A simple, bisection-based algorithm, commonly called the "box method," is employed to determine the nominal maneuver necessary to deliver the observatory to an orbit about L2. In this method, upper and lower bounds for the trajectory along the x-axis of the RLP frame are established. The RLP frame is centered on the Earth, with the +x-axis defined as the direction from the Earth toward L2, +z parallel to the Sun-Earth/Moon angular momentum vector, and +y completing the triad. Currently the box encompasses the space between 1,000,000 and 2,000,000 km along the +x-axis (in terms of Fig. 2, between 157 and 314 R_E along the +x-axis); L2 is located approximately 1,500,000 km from the Earth. The box method is based on targeting the appropriate maneuver duration to remain in the box. Initially, the guessed maneuver duration, starting at 0 seconds, is increased in 10 second increments until the trajectory achieves the lower 1,000,000 km boundary, enters the box, and then falls back towards the Earth. The maneuver duration is further increased in 10 second increments until the upper bound is exceeded; that is, the observatory's trajectory enters the box and then exits the upper 2,000,000 km boundary. Because achieving an LPO is highly sensitive to maneuver duration (orbits about L2 are known to possess unstable manifolds), the burn durations to initially achieve and exceed the lower and upper bounds of the box, respectively, are typically within 10 seconds of each other. Once the lower and upper durations for the MCC maneuver are established, a bisection algorithm is employed to determine the nominal maneuver duration such that the observatory stays within the 1,000,000 km box for 600 days (approximately three LPO periods). Once the nominal maneuver duration, Δt_b , is established for a notional MCC-1a, that maneuver is implemented using a maneuver duration of $0.95\Delta t_b$ in the simulation, along with incorporating various statistical modeling effects (discussed in future sections). Once the maneuver is executed in the simulation, the trajectory is propagated to the time of MCC-1b (launch + 2.5 days) and the targeting and execution process is repeated for MCC-1b, including the 95% hold-back strategy. The trajectory is then propagated to launch + 5.5 days, where the observatory SRP model is updated to reflected deployment of the sun shield. Propagation continues up to the MCC-2 epoch (launch + 30 days). The same targeting and execution algorithm is implemented, except the 95% hold-back approach is not employed for the execution of MCC-2. The maneuver duration is small enough such that any excess energy from statistical variations is not detrimental to achieving an LPO. After MCC-2, the trajectory is propagated another 21 days, at which point an impulsive maneuver scheme is implemented in the simulation to station-keep the orbit for 10.5 years. Note that two companion studies examine other mission design considerations: the propellant requirements for station keeping over the lifetime of the mission [1] and the launch window availability [2].

3. Propulsion Modeling

Before proceeding to the simulation, a proper propulsion model needs to be established in order to accurately model the three finite MCC maneuver. A description of propulsion modeling for this investigation follows. First, an overview of the propulsion system and the timeline for a single maneuver is presented. Next, the propulsion modeling assumptions for this study are outlined. These assumptions include a description of the acceleration components from the two types of thrusters on JWST, the expected maximum duty cycles from the attitude thrusters, attitude restrictions and the resulting effects on the maneuver direction, and description of thrust and Isp calculations for the thrusters as functions of cumulative on-time. Finally, the statistical variations that are employed in this study are described.

3.1 Propulsion System Overview

Two sets of thrusters comprise the observatory's propulsion system. The first is a set of Secondary Combustion Augmented Thrusters (SCATs) that are the main thrusters for the MCC maneuvers. The SCATs are bi-propellant thrusters and draw from two separate tanks for a hypergolic reaction. Two pairs of SCATs exist: one for MCC-1a and -1b, and one for MCC-2. The MCC-2 SCAT is also employed in station keeping throughout the life of the mission. Two pairs are required because the center of mass of the observatory changes between MCC-1b and MCC-2 because of the sun shield deployment; the thrust vector from a SCAT is directed through the center of mass at the time of that maneuver. Each pair is composed of a primary and a redundant thruster (the respective thrusters are coupled to the prime and redundant flight systems; only one system is on at a time). SCAT 1 and 2 are the primary and redundant pair for MCC-1a/b while SCAT 3 and 4 are the primary and redundant pair for MCC-2 and station keeping. For a given maneuver only one SCAT is on throughout that maneuver. The second set of thrusters is composed of eight Dual Thruster Modules (DTMs), each comprising of a primary and redundant Monopropellant Rocket Engine, 1 lbf, (MRE-1) thruster. A schematic of the propulsion system appears in Fig. 3. The MRE-1s consume hydrazine fuel only (and no oxidizer) from the same tank as the SCATs. The MRE-1s are subdivided into two sets: MRE-1s 1 through 4, which are directed generally along the observatory $-J3$ axis for pitch and roll control, and MRE-1s 5 through 8, which are directed radially about the $J3$ axis for yaw control [3]. A picture of the spacecraft bus with the body J frame and orientation of the SCATs relative to the J frame appears in Fig. 4. Together, the MRE-1s on-pulse throughout a maneuver to control the attitude. Because of the location and alignment of MRE-1s 1 through 4, any firings to control pitch and roll during a maneuver may result in an additional ΔV to the MCC maneuver. Therefore, thrust contributions from the MRE-1s must be included in the design of the MCC maneuver.

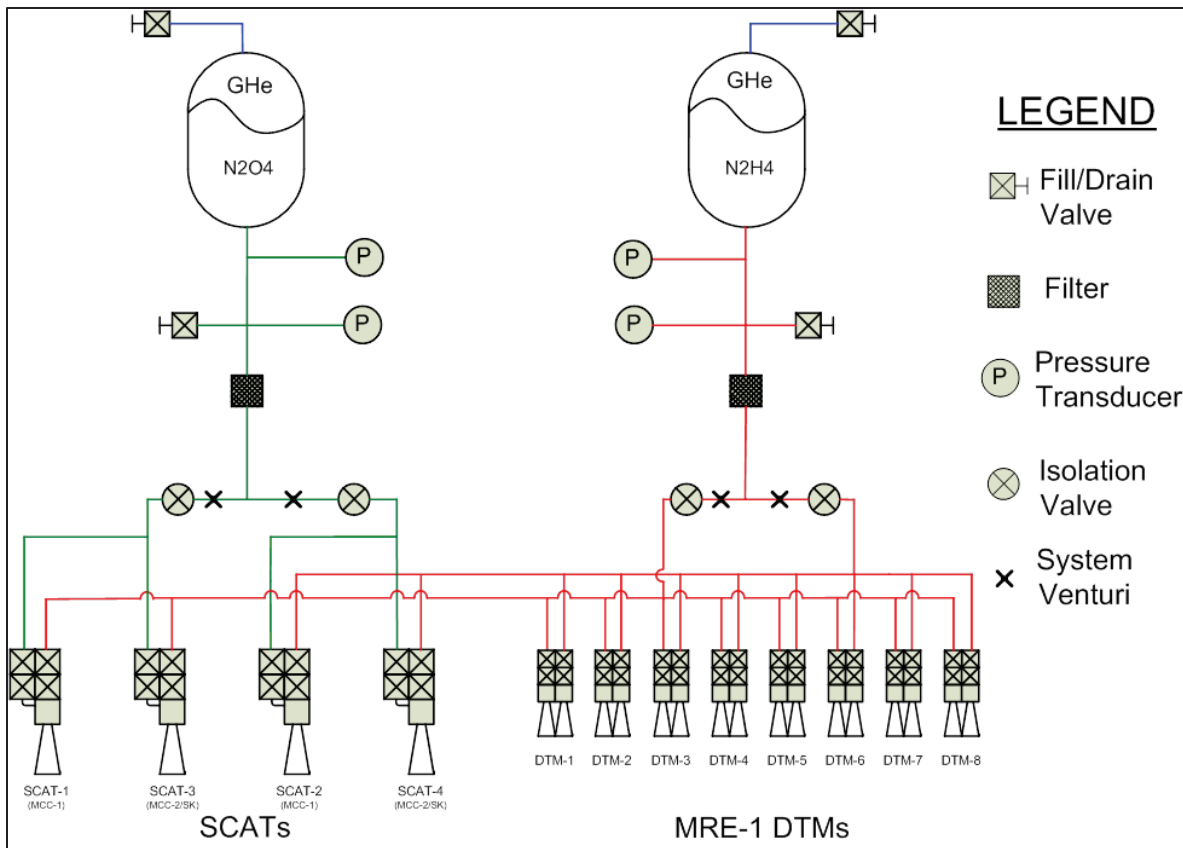


Figure 3. Schematic of the JWST propulsion system [4].

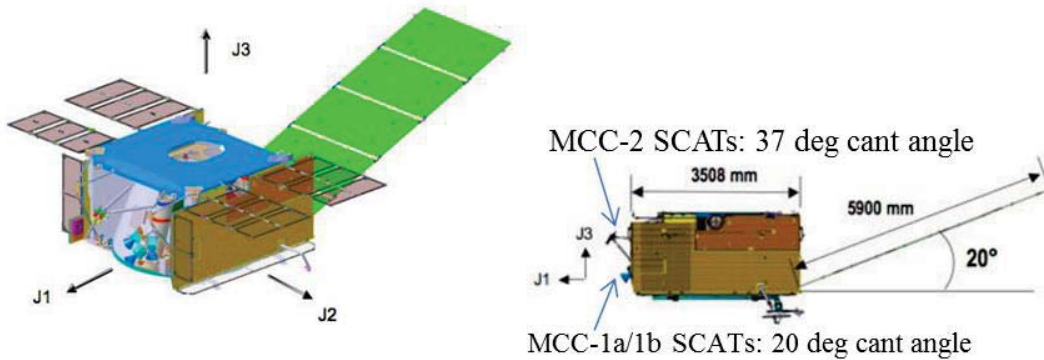


Figure 4. An independent view of the spacecraft bus showing the orientation of the body J frame along with the orientation of the SCATs relative to the spacecraft bus. The +J1 axis points in the general direction of the OTE boresight. The +J3 axis is roughly perpendicular to the multilayer sunshield and pointing parallel to the primary mirror (Image credit: jwst.nasa.gov)

Each MCC maneuver is composed of six steps [5].

1. First, the observatory begins in a nominal Attitude Control Subsystem (ACS) mode.
2. Second, the observatory slews to the burn attitude.
3. Third, the observatory transitions into ACS ΔV mode.
4. Fourth, the observatory performs the main burn using the SCATs and MRE-1s.
5. Fifth, the main burn ends and the MRE-1s perform a post-burn stabilization maneuver.
6. Finally, the observatory transitions back to its normal ACS mode.

Steps four and five are the only steps that contain thruster firings and, consequently, are the only times in which ΔV is added to the trajectory. In this investigation, only ΔV from the fourth step is incorporated into the simulation. The contribution from the post-burn stabilization maneuver (step five) is insignificant compared to any modeling errors during the main burn and is, thus, ignored in this analysis. However, during the long MCC-1a burn in step four, contributions from the MRE-1s to the ΔV may not be negligible and are thus included in maneuver modeling.

3.2 Propulsion Modeling Assumptions

A simple relationship between the thrust force from both sets of thrusters and mass of the observatory with the acceleration imparted on the trajectory from the MCC maneuver is

$$\mathbf{a}_b = \frac{1}{M} \left((1 + \xi \cdot \sigma_s) \mathbf{F}_s + \sum_{i=1}^8 (\eta_{b,i} DC_{b,i} \cdot \mathbf{F}_{m,i}) \right) \quad (1)$$

where M is the instantaneous mass of the observatory, \mathbf{F}_s is the thrust from the SCAT, and $\mathbf{F}_{m,i}$ is the thrust force from each of the MRE-1s. The $(1 + \xi \cdot 3\sigma_s)$ term allows for uncertainty in the magnitude of SCATs, where $3\sigma_s = 5\%$ and $\xi \sim N(0,1)$, where N is a normal distribution with mean 0 and a standard deviation of 1. The maximum effective duty cycle of the i^{th} MRE-1 throughout the maneuver is represented by $DC_{b,i}$. It is not expected that each MRE-1 will operate at its maximum duty cycle due to unmodeled attitude behavior during each maneuver, so a factor of $\eta_{b,i}$ is applied to each MRE-1, which $\eta_{b,i}$ conforms to some distribution. The current assumption is that $\eta_{b,i} \sim U(0,1)$, a uniform distribution between 0 and 1. Maximum-case duty cycles will be provided by the JWST attitude-control and propulsion subsystems. Notional values based on that analysis for MCC-1a/-1b and MCC-2 are listed in Tab. 1 (blank entries indicate that the value is zero). Additionally, after each maneuver a transition to a normal ACS mode exists prior to which the post-burn attitude is stabilized via MRE-1 thruster firings. The effective duty cycles are also listed in Tab. 1; however, as mentioned the post burn duty cycles are neglected in this investigation because of their insignificant contribution to the overall ΔV magnitude.

Table 1. Notional maximum MRE-1 duty cycles during MCC 1-a/b and MCC-2 (blank entries indicate that the value is zero)[5].

	MCC-1a/b		MCC-2	
	Burn	Post-burn	Burn	Post-burn
$DC_{b,1}$	0.013	0.003	0.001	0.029
$DC_{b,2}$		0.004	0.253	0.048
$DC_{b,3}$		0.005	0.119	0.033
$DC_{b,4}$	0.263	0.003		0.049
$DC_{b,5}$	0.043	0.006	0.101	0.007
$DC_{b,6}$		0.008		0.005
$DC_{b,7}$	0.043	0.006	0.101	0.007
$DC_{b,8}$		0.008		0.005

The thrust forces and specific impulse values (and, consequently, observatory mass) of the SCAT and MRE-1s vary throughout the maneuver as functions of tank pressures. In addition, the spacecraft does not contain any accelerometers to determine the achieved ΔV . Therefore, the only available controls for targeting a future condition along the JWST trajectory is the duration of the maneuvers, Δt_b , and the direction of the maneuver itself. The design of the JWST injection state is biased toward a low-energy condition in that the trajectory cannot go beyond L2. Energy is added at MCC-1a/b in that these maneuvers for targeting an LPO are implemented parallel (or as close to parallel as solar aspect angle constraints will allow) to the Earth-centered inertial (ECI) velocity vector. Burn angle constraints for MCC-1a/b and MCC-2 differ. The observatory has the capability to command burn angles from 5 degrees to 30 degrees, corresponding to sun pitch³ angles of -20 degrees to 5 degrees because the MCC-1a/b thrusters are approximately 10 degrees off the J2/J3 plane. For either MCC-2 or station keeping, the allowable commanded burn angles are in the range of 37.4 degrees to 90.4 degrees, corresponding to commanded sun pitch angles of 0 to 53 degrees [6].

Observatory pointing requirements during an MCC maneuver are decoupled from the maneuver model such that the ΔV is effectively along the axis of the SCAT used in the maneuver. Components of the thrust from the MRE-1s that are normal in direction to that of the SCAT may result in lateral motion relative to the axis of the SCAT used in the maneuver. The purpose of on-pulsing the MRE-1s is solely to ensure that the net thrust vector passes through the center of mass of the observatory. Because the unit vector from the location of the SCAT to the center of mass (which is variable because the CM changes throughout the maneuver and lifetime of the mission) is not necessarily parallel to the thrust direction of the SCAT employed during the maneuver (which is fixed), the *net* thrust direction is not necessarily parallel to the SCAT direction. Fortunately, the migration of the CM during MCC-1a/b is nearly along the SCAT thrust vector and subsequent maneuvers are relatively brief [7]. Therefore, the torque applied is fairly consistent throughout the maneuver. However, even with a “consistent” torque, a lateral component of the net thrust is possible. For the current analysis, this lateral motion is assumed to

³ Sun pitch measures the Sun direction from the $-J3$ axis about the $J2$ axis.

be negligible and the *net* thrust is directed along the unit vector of the SCAT employed in the maneuver; that is

$$a_b = \frac{1}{M} \left((1 + \xi \cdot \sigma_s) F_s + \sum_{i=1}^8 (\eta_{b,i} D C_{b,i} \cdot F_{m,i} \cos \beta_i) \right) \quad (2)$$

where $F_{m,i} \cos \beta_i$ accounts for the contribution from the i^{th} MRE-1 directed along the thrust vector of the SCAT employed for the MCC maneuver. Values for $\cos \beta_i$, the projection of the MRE-1s burn vectors onto that of a particular SCAT, are listed in Tab. 2. Recall that SCAT-1 and SCAT-3 are primary thrusters, while SCAT-2 and SCAT-4 are the respective redundant thrusters.

Table 2. Projection coefficient of each MRE-1s onto the respective SCAT burn vectors [8][9]

MRE-1	MCC-1a/b		MCC-2	
	SCAT-1	SCAT-2	SCAT-3	SCAT-4
1	0.76	0.78	0.42	0.43
2	0.92	0.94	0.94	0.95
3	0.94	0.92	0.96	0.95
4	0.79	0.77	0.43	0.42
5	-0.20	-0.25	-0.49	-0.52
6	0.05	0.00	0.37	0.34
7	-0.01	0.04	0.33	0.36
8	-0.26	-0.21	-0.53	-0.50

During the simulation, the thrust and ISP for the SCATs and the MRE-1s are calculated from a series of second order polynomials as functions of cumulative thruster on-times [4]. Throughout the simulation, the cumulative on-time of the thruster is stored in memory. The thrust and ISP are updated every 10 seconds of simulated on-time based on the current cumulative thruster on-time.

A maneuver duration restriction is placed on each of the three MCC maneuvers. MCC-1a, MCC-1b, and MCC-2 are restricted to maximum burn durations of 11,425 seconds, 2622 seconds, and 1301 seconds, respectively [4]. This restriction plays a crucial role in defining the potential launch windows as the maximum burn duration effectively limits the amount of ΔV available to the observatory.

3.3. Monte Carlo Simulation Variations

Following the goal of estimating the ΔV distribution, the MCC Monte Carlo simulation employed for this study allows for statistical variations in several aspects of the model including launch vehicle injection state, position and velocity state at the epoch of each MCC maneuver based on the quality of the orbit determination (OD) solution, SCAT thruster performance, MRE thruster performance, and attitude pointing during the execution of the three MCC maneuvers.

The launch vehicle injection state and the quality of the OD solution will affect the maneuver targeting algorithm as those two variations will affect the pre-maneuver state. The SCAT and MRE performance and attitude knowledge will alter the achieved ΔV from the nominal targeted ΔV .

At the beginning of the simulation, one of three launch vehicle injection states provided by Arianespace is selected along with a specific launch epoch. The three injection states correspond to apogee heights of 1.02, 1.06, and 1.10e6 km, respectively. Potential launch epochs span from October 2018 to December 2019 at any time between 11:30 and 14:00 UTC. The current focus is an October 2018 launch. Using the injection state correlation matrix and standard deviation provided by Arianespace [10], the nominal injection state is perturbed to simulate possible injection errors.

The true state is then propagated to the next MCC maneuver. The next component of the Monte Carlo tool models the possible position and velocity errors in maneuver planning associated with realistic orbit determination solutions. At the time of each MCC maneuver, the position and velocity are randomly perturbed from their true states per the appropriate navigation covariance matrix. This navigation nominal state (in error from the true state) is employed to design the corresponding MCC maneuver.

As discussed in the previous section, the performance of the SCATs and the MRE-1s are modeled via a normal distribution for the SCATs and a uniform distribution for the MRE-1s. The 3σ performance of the SCAT thrusters (5% in this analysis) is defined as a user input. The Monte Carlo simulation draws a random value from Gaussian distribution and applies a thrust scale factor to the SCAT accordingly. The thrust scale factor is meant to simulate possible hot or cold performance of the SCATs. Similarly, the statistical variation in the MRE-1s employs a uniform distribution in applying a scale factor to the duty cycles for individual MRE-1s.

The final variation is the attitude pointing during the maneuver. The attitude of the observatory is required be known to within five degrees (3σ) in roll, pitch, and yaw at the time of the maneuver.⁴ At the time of the maneuver, the thrust vector is applied as close as possible to the inertial velocity vector while still maintaining the sun pointing requirements. Once the thrust vector has been established, roll, pitch, and yaw are modified independently from a normal distribution with the five degree requirement as the 3σ variation to statistically model the attitude knowledge error at the time of the maneuver.

4. Parallel Architecture

While reasonable attempts are made to ensure that the propulsion system, attitude control system, and other aspects of the observatory are modeled correctly when formulating the design of the MCC Monte Carlo analysis tool, mission designers are aware of and appreciate the need for models and assumptions to change as the design of other subsystems evolve. Furthermore, with each change to other subsystems, propellant budget analyses will need to be regenerated,

⁴ The attitude knowledge requirements were discussed during a technical exchange between the flight dynamics team and Jon Hammann.

and simulations may be performed many times up until launch. Therefore, the MCC Monte Carlo analysis tool is designed to be modular and robust to changes between trials. Moreover, incorporating task parallelism greatly reduces the run time for a Monte Carlo analysis based on a particular set of assumptions.

In task parallelism each thread performs a completely different task on the same or different sets of data. The more common type of computing parallelism is called data parallelism, where the same calculation is performed on the same types of data at the same time. Rarely employed for Monte Carlo studies in space-flight mechanics, task parallelism is exploited in this investigation of the JWST MCC propellant budget. Each portion of the mission is represented with modular code sets that can be changed for individual analyses without compromising the overall integrity of the code. Furthermore, task parallelism provides the ability to view the results as they are generated, one-by-one, rather than waiting for large sets of data to be produced. Finally, task parallelism allows for tasks to be broken down into small pieces, allowing nodes to opt in and out of the processes without losing large amounts of the computed data.

The Python programming language is employed to manage the parallel architecture of the Monte Carlo tool. Python allows for quick development because of its intuitive interpretation architecture, multiprocessing library, and its ability to access the astrodynamics libraries and tools of the commercial-off-the-shelf (COTS) product FreeFlyer via socket connections. This architecture allows a user to execute up to as many instances of FreeFlyer at a time as there are processor cores in the computer.

The next step to building a parallel architecture is to parallelize the simulation over multiple compute nodes. Nodes are able to opt in and out of a simulation without any loss of data and, if something should happen to one of the nodes, results from that node are not lost, but re-trialed on another node. This functionality helps complete the simulations effectively when running in a computer lab environment where there are many idle computers but at any given time one or many may be taken away. This architecture also lends itself to a cloud computing environment, which is discussed shortly.

Another Python package, Celery, provides a robust messaging system that controls messages on a Publisher-Subscriber type relationship. Celery is a simple, flexible, and reliable distributed system to process vast amounts of messages, while providing the operations with the tools required to maintain such a system. Celery also provides ways to monitor and manage the Monte Carlo system which was developed using Celery's application programming interface (API).

The FreeFlyer scripts that represent different segments of the trajectory are sequenced to handle a single element of JWST's lifetime trajectory and draw the appropriate variations for each perturbation. These instantiation of these scripts responds to a single incoming message and returns the result in the form of another message. Tasks are written in Python to interpret a Celery message and provide it to an instance of FreeFlyer that is waiting for the message. The results are uploaded to the server in the form of the second message, which is waiting to be retrieved by the messaging system. From the user's point of view, all of the individual Monte Carlo trials are sent to the server in the form of messages. Workers listening to a particular message queue wait to handle those messages. The results are then sent to another messaging

queue that the user is monitoring for incoming result messages. For a particular node to opt out of the system, a simple command to stop subscribing to the message queue is all that is required. The node finishes the work that it is performing and sends its final results back to the messaging system. If no workers are available, the messages are not lost and work may resume when more workers are brought back online. The resultant messages also benefit from this durable system: results are not lost when workers quit performing; they are stored until the user retrieves them up. A visual representation of the task distribution system appears in Fig. 5.

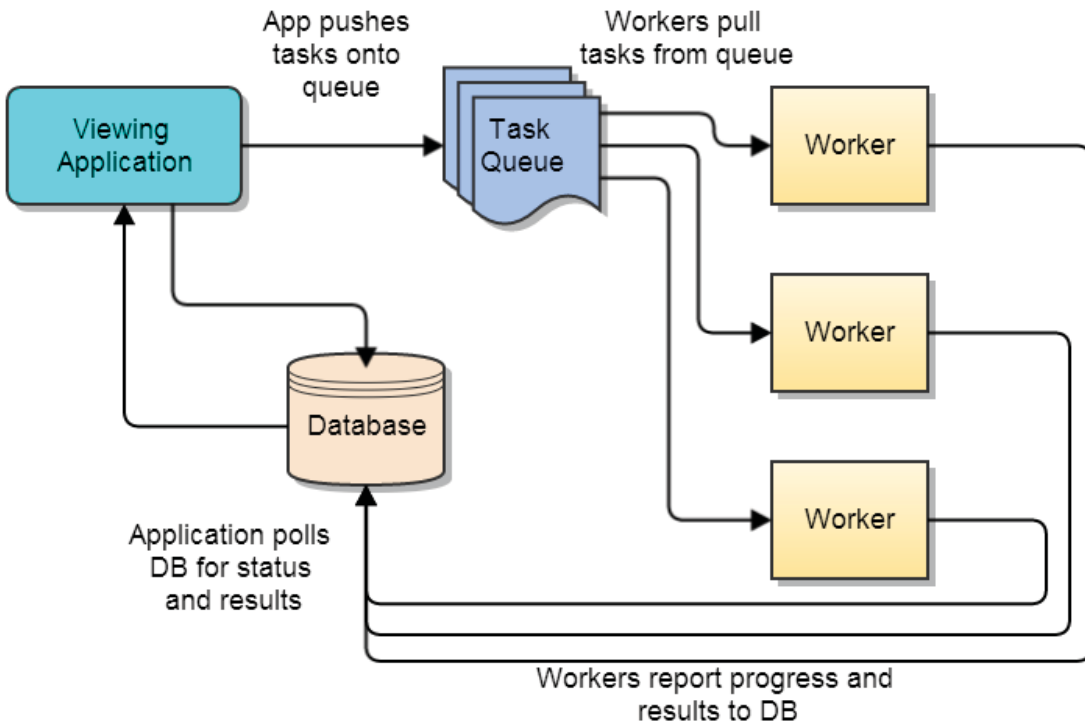


Figure 5. The viewing application pushes user defined tasks into a messaging system provided by the Python package, Celery. The messaging system distributes tasks to available workers. Each worker is an instance of FreeFlyer running on a single CPU core that models the lifetime trajectory. Once the simulation is complete, the results are reported back the database. Celery provides way to monitor and manage the results from the Monte Carlo simulation.

Celery integrates with many industry-standard queue systems. A local Rabbit-MQ system is employed in this investigation, but Celery also has the ability to exploit Amazon Web Services (AWS) features as a global messaging system. Future functionality includes the ability to integrate the message distribution system into a cloud-based system. A first step is to use the AWS Simple Queue System (SQS) to broker the messages between nodes. The SQS allows for the messages to be shared across the internet. Encrypted and encased in the AWS GovCloud, the messages are secured in a way that only a restricted few compute nodes have access to the messages. Coupled with AWS Simple Storage Solutions, users are able to access the results of the simulations from anywhere and are able to configure their FreeFlyer-licensed machine to dedicate a few worker cores to Monte Carlo analyses when their computers are idle. This

capability is anticipated in future versions of this analysis tool and is expected to require minimal code changes.

5. Initial Results from the MCC Monte Carlo Framework

Having the ability to model the injection state, propulsion system, attitude knowledge, and OD errors allows for detailed study into the potential ranges propellant consumption that are possible for the three MCC maneuvers. This section highlights three analyses that assess the necessary propellant budget for the MCC maneuvers. The first analysis examines the wide range of MCC-1a ΔV magnitudes and maneuver durations possible because of launch vehicle injection errors. The second example demonstrates the uncertainty in the propulsion performance and the downstream implications of these uncertainties in future MCC maneuvers. The final example quantifies the additional ΔV provided by the attitude modeling thrusters and the implications the additional ΔV can have on maneuver planning for each of the MCC maneuvers.

5.1 Launch Vehicle Injection Errors

The first question addressed in this analysis is the effect of the launch vehicle injection dispersions on the magnitude of MCC-1a. As described earlier, Arianespace supplies three nominal injection states along with a correlation matrix and standard deviation that characterizes the possible launch vehicle dispersions. The launch vehicle injection errors are the largest contributor to the uncertainty in maneuver planning process. The magnitude of the first MCC maneuver is strongly correlated to the energy provided by the launch vehicle. Using the Monte Carlo framework established in the preceding sections to incorporate the launch vehicle statistical variations, the range of ΔV required to insure a successful LPO orbit are analyzed based on 1000 Monte Carlo runs. The propulsion system, OD solutions, and attitude knowledge are modeled nominally. The only statistical variation for this example is the launch vehicle dispersions based on the Arianespace-provided data. The launch epoch employed for this example is October 01, 2018, 13:45:00 using the 1.10e6 km injection state. The results for this Monte Carlo simulation are provided in Fig. 6 and 7. Figure 6 demonstrates the expected Gaussian distribution of the MCC-1a ΔV resulting from the launch vehicle injection dispersions.

For the representative launch epoch of October 01, 2018 at 13:45:00 UTC, the expected specific energy from the launch vehicle is $-0.35586 \text{ km}^2/\text{s}^2$ corresponding to a nominal MCC-1a ΔV of 17.617 m/s. For this particular example, the linear relationship between the achieved injection state energy and the achieved MCC-1a ΔV is evident in Fig. 7. The amount of energy provided by the launch vehicle is strongly correlated to the amount of ΔV required for MCC-1a. The spread in 3σ MCC-1a maneuver duration ranges from a nominal 3865.57 seconds to approximately ± 3900 seconds. The 3σ specific energy distribution is approximately $\pm 0.04 \text{ km}^2/\text{s}^2$ which equates to roughly ± 17 m/s of ΔV from the nominal MCC-1a ΔV magnitude.

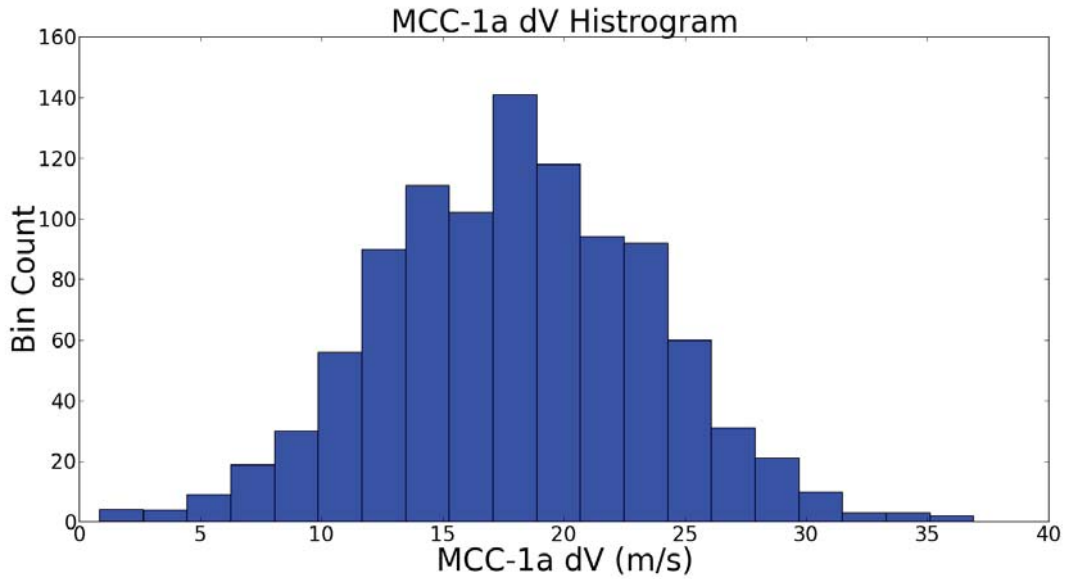


Figure 6. The variation in required MCC-1a ΔV reflects the Gaussian distribution used to model the injection state perturbations.

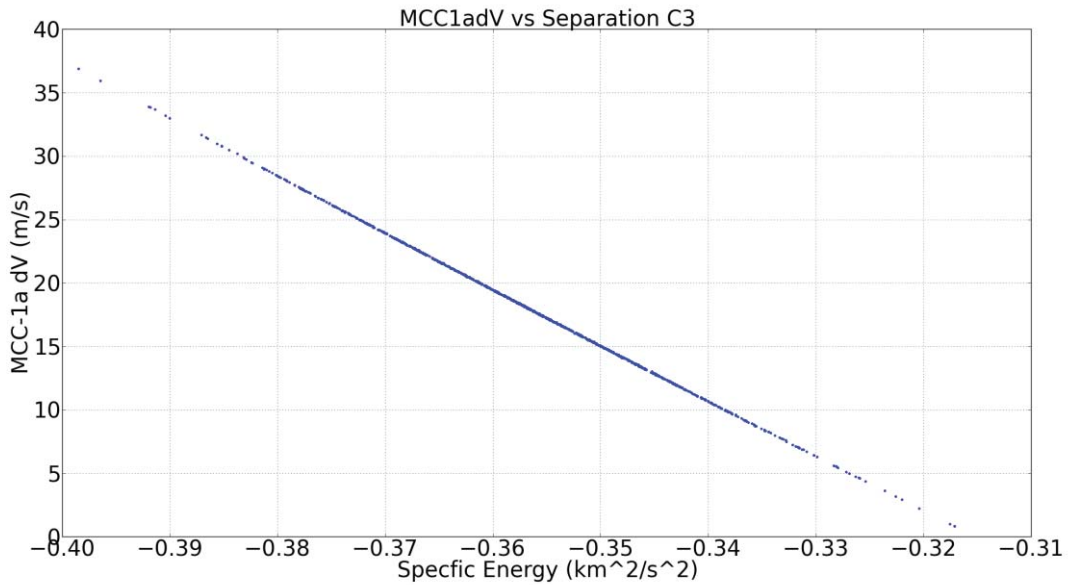


Figure 7. The expected linear relationship between the spread of injection states that the launch vehicle can provide and the resulting ΔV required for MCC-1a.

Understanding the possible variation in ΔV for MCC-1a due to the launch vehicle injection errors is crucial in mapping the launch window for JWST. The epoch provided in this example was selected because the nominal specific energy provided by the launch vehicle places the observatory in a state such that extreme perturbations to the injection state will still result in successful trajectories. For another launch epoch, it is entirely possible that a nominal injection state will correspond to a physically achievable maneuver duration by the propulsion system; however, the errors from the launch vehicle could result in an irrecoverable state through two possibilities: the errors from the launch vehicle provide too much energy and the observatory escapes the L2 region or the launch vehicle does not provide enough energy and the finite amount of ΔV onboard is not sufficient for the observatory to reach L2. In the example detailed above, the 3σ maximum maneuver duration required as a consequence of a low injection state is 8537 seconds, which is only 2888 seconds smaller than the maximum allotted maneuver duration of 11425 seconds. Given that the spread in 3σ maneuver durations is approximately ± 3900 seconds, it is plausible that specific launch epochs and their associated nominal injection states require a duration for the MCC-1a maneuver beyond the maneuver duration limit when incorporating 3σ dispersions. In these cases, observatory's trajectory would not possess enough energy to reach L2. The opposite is possible as well. The launch vehicle could place the observatory on a trajectory in an unrecoverable state beyond L2 and beyond the ability of any maneuver to rectify the trajectory.

5.2 Propulsion Performance

A second analysis focuses on the variation in the three MCC maneuvers based on performance of the propulsion system. As part of the launch vehicle injection error analysis described in the previous section, the performance of the SCATs and MRE-1s is nominal for each maneuver. This analysis incorporates the effects of non-nominal performance of the propulsion system. Trending data from maneuver operations is often necessary in order to accurately predict the performance of the propulsion system. However, as the MCC maneuvers are both mission critical and performed without any calibration, trending data is not and will not be available. The results from this analysis assist in establishing the performance of the propulsion system.

As stated in the propulsion modeling section, the thrust and the ISP profiles for the SCATs and MRE-1s are updated every 10 seconds of simulated on-time during the propagation using second order polynomials that are functions of thruster cumulative on-time. The statistical model for the SCAT performance employs a normal distribution with a 3σ standard deviation of 5%. The necessary attitude corrections provided by the MRE-1s are unknown because the attitude variations throughout the maneuver are unknown. A coefficient returned from a uniform distribution between 0 and 1 is applied to the maximum duty cycle highlighted in Tab. 1 to model potential variation in the ΔV contribution from the MRE-1s during the maneuver.

The box method is based on the assumption that the propulsion system will perform nominally when targeting the burn duration required to place the observatory into an operational LPO. Once a maneuver duration is determined (after applying the 5% hold back of the designed maneuver duration to mitigate overshoot), the simulation executes the targeted maneuver with the statistical variations from the propulsion model. If the executed maneuver burns hot, the resulting trajectory is unlikely to exceed the LPO and be lost in deep space. Subsequent

maneuvers bring the trajectory into the LPO. The following example employs a launch epoch of October 18, 2018, at 12:30:00 using the 1.06e6 km injection state. Under a nominally performing propulsion system (i.e., no statistical variations are applied), the targeted maneuver durations and corresponding ΔV for the three MCC maneuvers are listed in Tab. 3.

Table 3. Targeted MCC maneuver durations and associated ΔV for a launch epoch of Oct 18, 2018 at 12:30:00 UTC using the 1.06e6 km injection state.

	Maneuver Time	Nominal Duration (seconds)	Nominal ΔV (m/s)
MCC-1a	Launch + 0.5 days	4952.28	22.279
MCC-1b	Launch + 2.5 days	455.68	1.967
MCC-2	Launch + 30 days	149.40	0.712
Cumulative	--	5557.36	24.958

As expected, the majority of the ΔV is applied during MCC-1a. When performing a simulation using a nominal propulsion system, MCC-1b acts purely as correction for the 5% hold back in MCC-1a. MCC-2 corrects for the 5% hold back in MCC-1b. Once propulsion performance errors are introduced into the simulation, MCC-1b and MCC-2 become statistical correction maneuvers in addition to the 5% hold back correction. The histogram appearing in Fig. 8 shows the potential variation in MCC-1a ΔV when the propulsion performance errors are incorporated into the simulation. This histogram is based on 1000 simulations. The maneuver duration is the same for each of the 1000 Monte Carlo trials of the MCC-1a maneuver. The variation in ΔV arises only from the statistical errors characterizing the propulsion system.

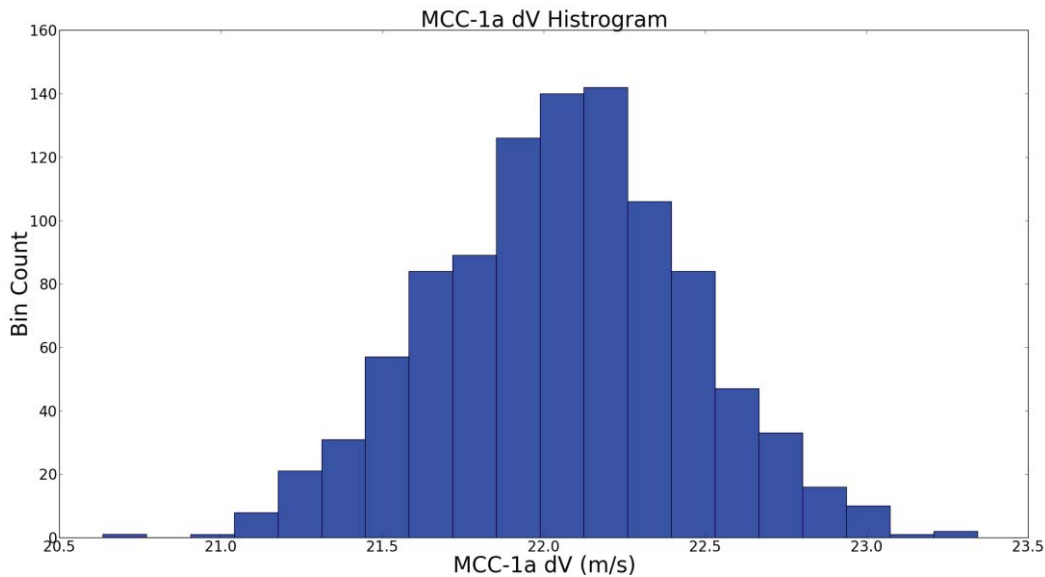


Figure 8. Variation in MCC-1a ΔV due to statistical variation in propulsion performance. The nominal ΔV is 22.279 m/s while the statistical mean of the data set is close at 22.057 m/s.

For this particular data set, the mean ΔV for MCC-1a is 22.057 m/s, which matches closely with the nominal ΔV of 22.279 m/s from Tab. 3. The SCATs are the primary contributor to the ΔV for each MCC maneuver. Thus, it is expected that the $\pm 5\%$ three-sigma performance of the SCATs drive the ΔV distribution seen in Fig. 8. Based on a simple back of the envelope calculation, a 5% error in either direction about the nominal would result in a 5% cold ΔV of 21.17 m/s and a 5% hot ΔV of 23.39 m/s. A visual inspection of Fig. 8 confirms that a majority of the ΔV distribution falls within the range established by that calculation. While the MRE-1s do contribute to the maneuver performance, it appears (as expected) that the SCATs contribute the majority of the ΔV dispersion.

The effects of propulsion performance errors is apparent when applied to the execution of MCC-1b, as this maneuver serves two purposes: it supplies an additional ΔV boost to make up the 5% hold back from the previous maneuver, and it provides a statistical correction to compensate for performance from the previous maneuver. For MCC-1a, the duration for the executed maneuver is the same for each Monte Carlo run, as the targeting algorithm determines the maneuver duration using a nominal propulsion system based on the same pre-maneuver state. The subsequent nominal MCC-1b maneuver duration determined by the targeting algorithm that is necessary to place JWST into the LPO is strongly dependent on the performed MCC-1a maneuver, as apparent in Fig. 9. A tight linear relationship between the achieved ΔV from MCC-1a and the resulting maneuver duration necessary for MCC-1b are also apparent in the figure. Simply put, a lower achieved ΔV from MCC-1a results in a higher targeted maneuver duration for MCC-1b. For MCC-1b, each of the simulations has a unique pre-maneuver state because of the propulsion performance from MCC-1a. The variation in the pre-MCC-1b maneuver state across the Monte Carlo samples causes the wide range of necessary maneuver durations, as apparent in Fig. 10. The resulting variation in MCC-1b ΔV , appearing in Fig. 11, differs from the shape of the histogram in Fig. 10 as a consequence of the combination of variation in MCC-1b targeted maneuver duration and propulsion performance modeled during the execution of MCC-1b itself.

For the setup in this analysis, the duration of MCC-1a is always the same; however, the duration of MCC-1b varies. The targeted maneuver duration for MCC-1b is no longer a single value. This additional variation appears in Fig. 12 by comparing the targeted maneuver duration and achieved ΔV for MCC-1b. The achieved ΔV for a given maneuver duration is not perfectly linear, and the fluctuation in required ΔV because of the cumulative effects is apparent: variation in the executed ΔV to reach L2 is a function of propulsion performance from MCC-1a and MCC-1b.

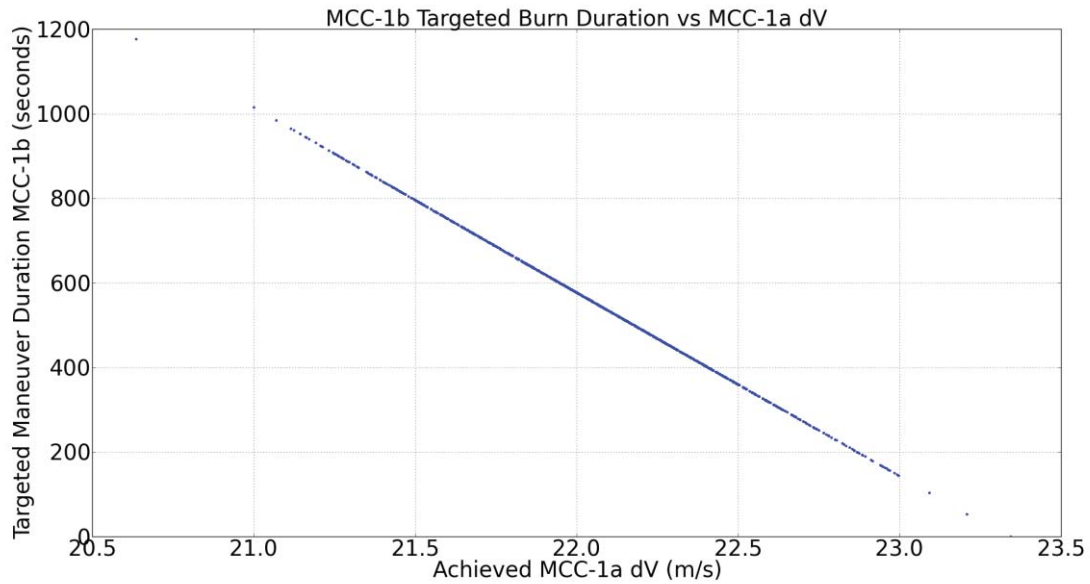


Figure 9. The tight linear relationship between the achieved ΔV for MCC-1a and the resulting targeted maneuver duration for MCC-1b. The propulsion performance for MCC-1a is the only statistical variation up to this point in the simulated trajectories.

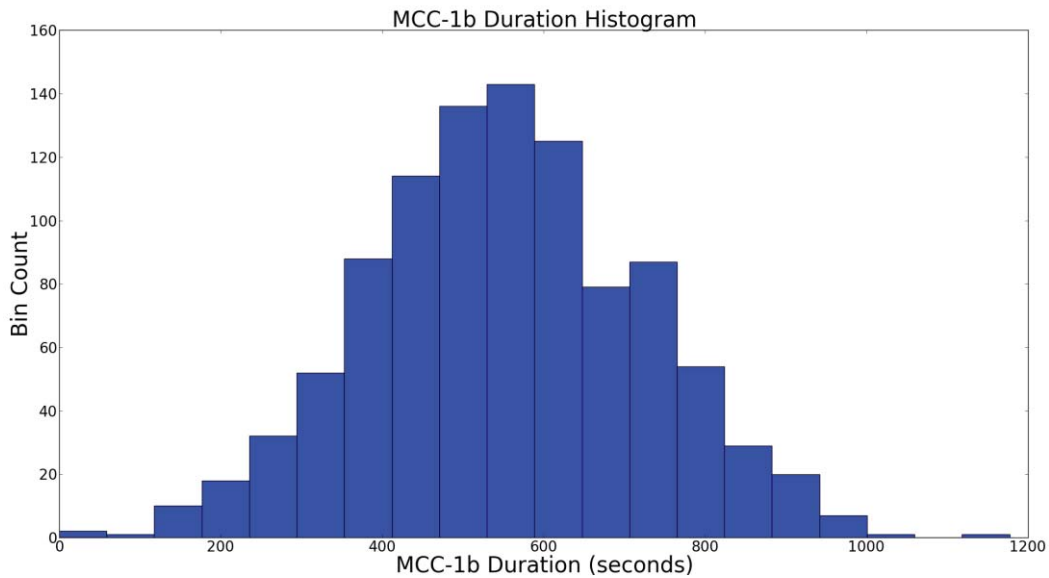


Figure 10. Variation in MCC-1b targeted maneuver duration. The variation in the targeted maneuver duration results from two effects: additional ΔV required to make up the hold back from MCC-1a, which is between 0 and 10% of the targeted MCC-1a burn duration (3σ), and the statistical correction to compensate for MCC-1a propulsion performance.

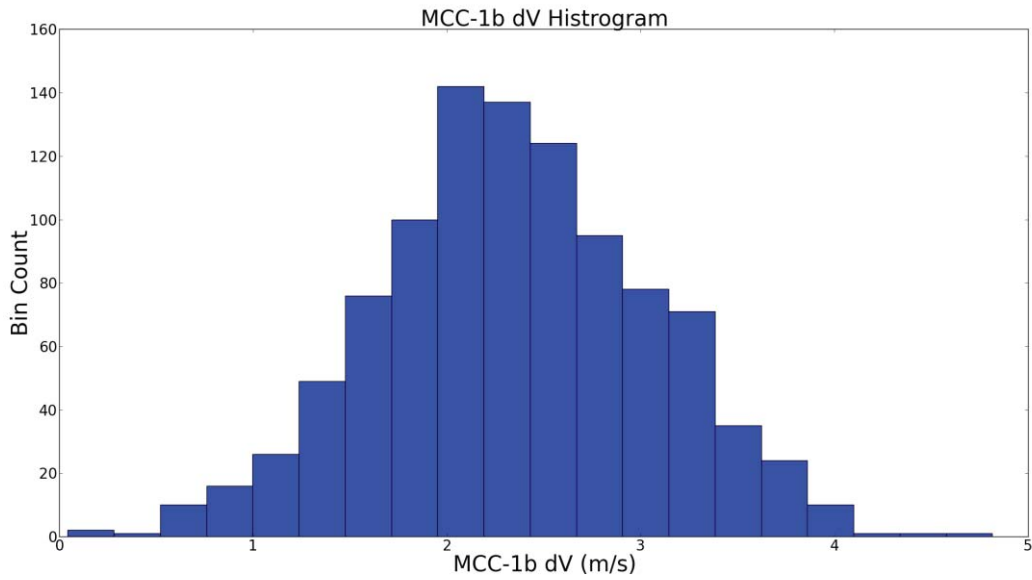


Figure 11. Variation in MCC-1b achieved ΔV . The shape of the histogram differs from the MCC-1b targeted maneuver duration as the propulsion performance causes variation between the targeted and achieved results.

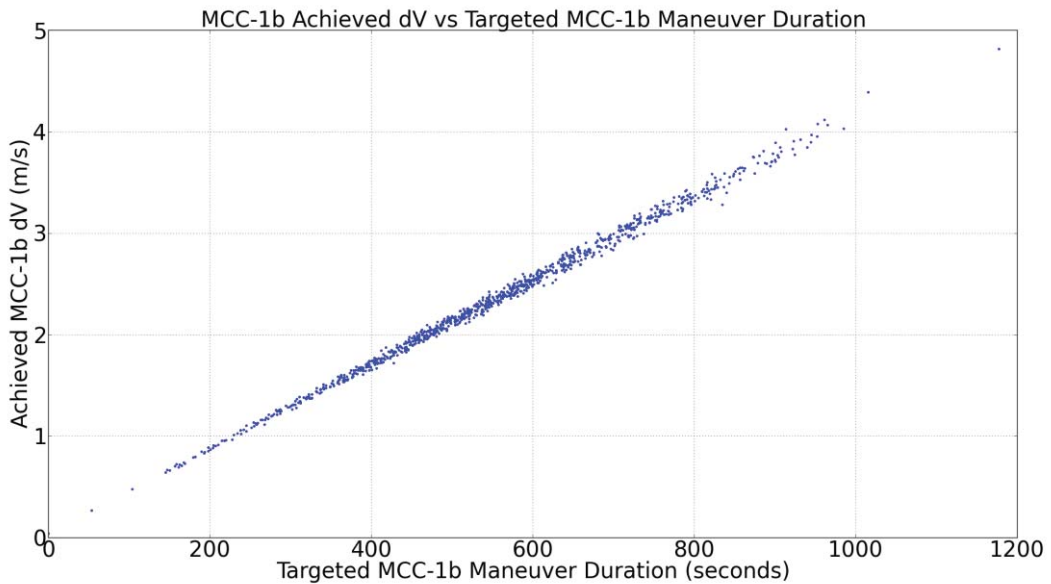


Figure 12. The linear, but dispersed, relationship between the targeted MCC-1b maneuver duration and the achieved ΔV for MCC-1b due to cumulative effects from MCC-1a and MCC-1b propulsion performance.

The relationship between MCC-2 and MCC-1b is more complex than the relationship between MCC-1a and MCC-1b: MCC-2 incorporates a combination effect of propulsion performance from both MCC-1a and MCC-1b. MCC-2 is the smallest of the three MCC maneuvers and is effectively the first station keeping maneuver. Of particular interest in Fig. 13 is the spread of maneuver durations possible for MCC-2. Figure 9 shows a similar comparison between MCC-1a achieved ΔV and the targeted maneuver duration for MCC-1b, but the relationship is solely dependent on the achieved ΔV from MCC-1a. The linear relationship of the ΔV of MCC-1b to that of MCC-2 is apparent, but the result is more dispersed because of the combination of propulsion performance from MCC-1a and MCC-1b. Up to this point in the trajectory simulation, most of the histograms appeared Gaussian, matching the statistical modeling for the SCATs. The dispersion of the MCC-2 maneuver durations and associated ΔV s that accounts for the cumulative effects of the preceding maneuvers is non-Gaussian and possesses a skewness, which is apparent in Figs. 14 and 15, respectively.

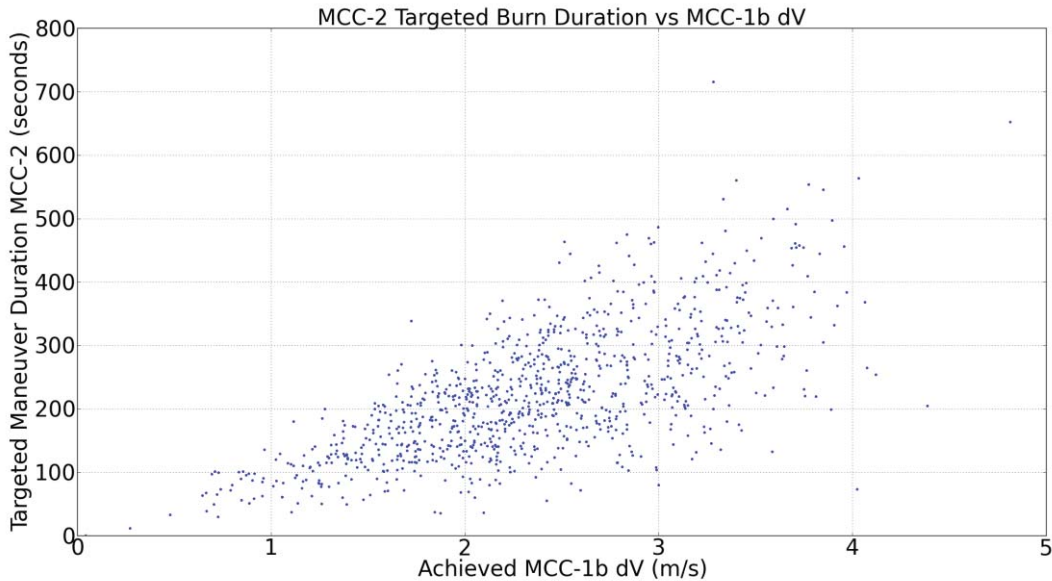


Figure 13. The distribution between the achieved MCC-1b ΔV and targeted maneuver duration for MCC-2 no longer exhibits the tight linear relationship shown between MCC-1a achieved ΔV and the targeted maneuver duration for MCC-1b.

Overall, the functionality for the propulsion system highlights the range of potential ΔV for each MCC maneuver. One important result from this analysis is that finding a successful trajectory is possible for these scenarios given the current propulsion modeling, thus validating that the propellant budget is robust to propulsion performance perturbations. For other scenarios, specifically certain launch opportunities, finding a suitable trajectory may not be possible. In particular, scenarios that push the boundaries of the ΔV budget, both the low and high end, could potentially fail to achieve an operational orbit. The current framework allows for further study into the performance of successful launch opportunities and mid-course corrections with the combination of the effects from the launch vehicle injection errors and the propulsion performance.

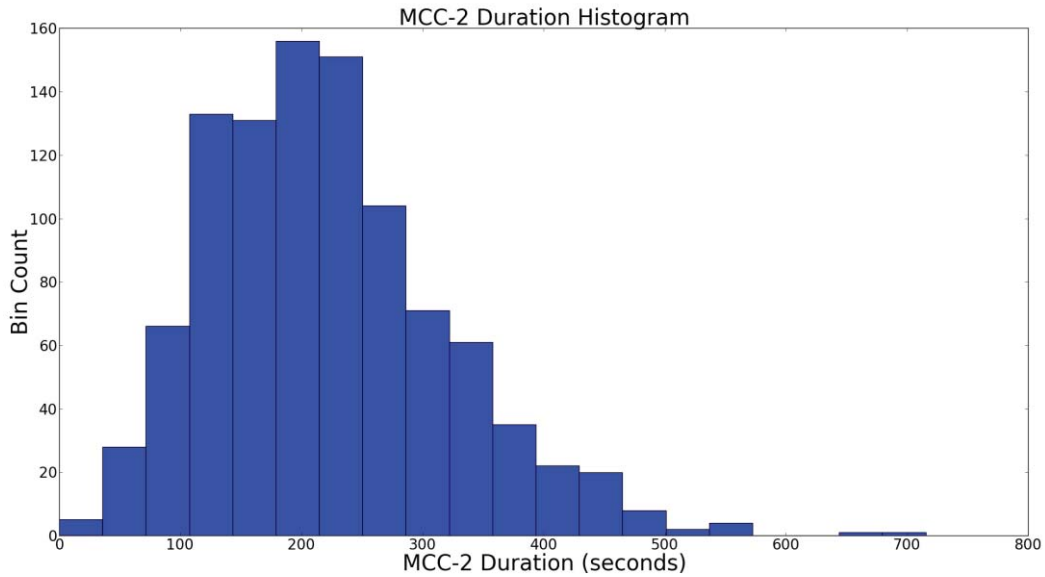


Figure 14. Histogram showing the spread of targeted MCC-2 durations. The skewness of this data demonstrates the results of compounding maneuver performance from MCC-1a and MCC-1b.

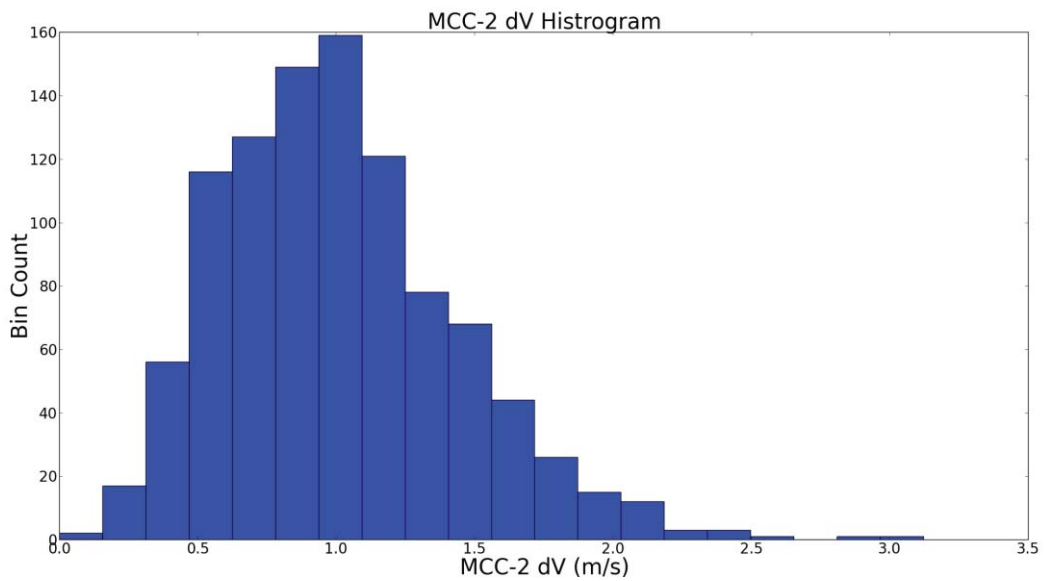


Figure 15. Histogram showing the spread of achieved ΔV for MCC-2. Once again, the skewness is a factor for the compounding propulsion performance between all three MCC maneuvers.

5.3 Minor ΔV Contribution from the MRE-1s

In the previous section, a quick back of the envelope calculation indicates that the performance of the SCAT is the contributing factor in the range of achieved ΔV for MCC-1a. While the SCATs dominate the variation in propulsion performance, the MRE-1s do contribute ΔV to the maneuver and must be accounted for in determining the maneuver duration for each MCC. The SCATs are approximately 10 times stronger than the MRE-1s; however, there are potentially eight active MRE-1s. Tables 1 and 2 list the maximum duty cycles and the projection, respectively, of each MRE-1 burn vector onto the various SCAT burn vectors. The projected components contribute to the cumulative ΔV in a maneuver. An approximation of the MRE-1 contributions is determined by a summation of the individual MRE-1s contribution through a multiplication of the duty cycle, projected onto the particular SCAT burn direction, and relative strength compared to the SCAT (the thrust provided by an MRE-1 is approximately 10% of a SCAT). The summation reveals that the MRE-1s contributes an approximate 2% additional ΔV for MCC-1a and -1b and approximately an additional 3.5% for MCC-2. The difference occurs because different SCATs are used for MCC-1a/b and MCC-2.

A more robust answer for the contribution of the MRE-1s is determined from the Monte Carlo simulation framework. Two different trajectories are employed, one in which the propulsion system includes the MRE-1 contributions and one in which the MRE-1s are turned off. Based on a launch epoch of October 10, 2018, at 12:30:00 UTC and the 1.06e6 km injection state, the difference in maneuver duration and ΔV between the two scenarios appears in Tab. 4.

Table 4. Maneuver duration and ΔV comparison demonstrating the slight, but significant, impact the MRE-1s have during the maneuver planning process.

Duration (seconds)	MCC-1a	MCC-1b	MCC-2	Cumulative
SCATs Only	5068.83	466.22	155.17	5690.22
SCATs and MRE-1s	4952.28	455.68	149.40	5557.36
Percent Difference	-2.300	-2.261	-3.719	-2.335
ΔV (m/s)	MCC-1a	MCC-1b	MCC-2	Cumulative
SCATs Only	22.290	1.960	0.711	24.961
SCATs and MRE-1s	22.279	1.967	0.712	24.958
Percent Difference	-0.05	0.357	0.141	-0.012

The ΔV comparison between the SCATs-only scenario and the combination of the SCATs and MRE-1s is much less than 1%. The small, almost negligible, difference makes sense given that the same ΔV is required for LPO insertion regardless of propulsion system setup. The maneuver duration, however, differs significantly. For the example in Tab. 4, the maneuver duration is reduced by approximately 132 seconds after incorporating contribution of the MRE-1s into the propulsion modeling. This difference is roughly 2.3% of the cumulative on-time for the thrusters. Further insight arises when breaking down the cumulative effect into individual maneuvers. The percent difference for each individual maneuver matches the rough estimate of 2% for MCC-1a/b and 3.5% for MCC-2. Given that the maneuver duration is the only control variable

available for maneuver planning, highlighting the MRE-1s small, but relevant, contribution to each MCC maneuver is a significant result. Proper modeling of the propulsion system is crucial to developing a model to accurately plan the maneuver duration for each MCC.

7. Conclusions and Future Work

A Monte Carlo simulation is developed to validate and determine the robustness of the ΔV budget arising from statistical variations that occur during maneuver execution. The current version of the Monte Carlo tool incorporates the following features: statistical modeling of the launch vehicle dispersions provided by the Ariane 5 rocket, quality of the OD solutions that supplies the pre-maneuver position and velocity at each MCC epoch, statistical variation in the SCATs and MRE-1s performance, and the attitude knowledge at the time of each MCC maneuver. A system employing FreeFlyer as the flight dynamics software in conjunction with Python and Celery to act as a message distribution and collection service allows for optimized parallel processing to facilitate Monte Carlo simulations in a timely manner.

Three specific analyses are presented that provide an initial assessment of the implications of the various statistical modeling effects on the launch window and ΔV budget. First, the effects of the launch vehicle dispersion on the magnitude of MCC-1a are analyzed. Given the large spread in maneuver ΔV , it is possible that other epochs may or may not achieve an operational LPO, specifically launch epochs that require a ΔV that pushes the upper boundary of the maximum maneuver duration. The second analysis focuses on validating the robustness of the ΔV budget based on the SCAT and MRE-1s performance during each of the MCC maneuvers along with the downstream impact to the later MCC maneuver. Given a nominal injection state, the uncertainty in the SCATs' performance is the significant contributor to the variations in the propulsion performance. As the propulsion performance errors accumulate throughout the trajectory, the variation in the later MCC maneuvers become larger to compensate for the compounding errors. The third and final analysis presented in this paper highlights the slight, but significant, impact that the MRE-1s contribute toward the duration of maneuver execution. Even though the MRE-1s only reduce the overall durations of MCC-1a/1b by 2% and by 3.5% for MCC-2, incorporating their contribution into maneuver planning. The spacecraft commands a maneuver duration, not an achieved ΔV . As such, a well-understood propulsion system and ensuring that the ΔV budget is robust to propulsion performance errors is crucial.

Future work includes extending the Monte Carlo execution framework to incorporate the benefits of the AWS GovCloud to help streamline the task distribution system. In addition the fidelity of the propulsion model will continue to be updated to reflect accurate statistical variations in the performance of the SCATs and MRE-1s. Eventually, a Monte Carlo simulation incorporating all of the potential statistical variations will be conducted to help validate the ΔV budget and the robustness of the maneuver planning strategy.

8. References

[1] Dichmann, D, Alberding, C, Yu, W, "Stationkeeping Monte Carlo Simulation for the James Webb Space Telescope". 24th International Symposium on Space Flight Dynamics (ISSFD). Laurel, Maryland, MD, USA, 2014.

- [2] Yu, W., Richon, K., “Lanch Window Trade Analysis for The James Webb Space Telescope”. 24th International Symposium on Space Flight Dynamics (ISSFD). Laurel, Maryland, MD, USA, 2014.
- [3] Gidanian, D. 7.0. ACS design & analysis: Thruster Configuration and Modeling. In *James Webb Space Telescope (JWST) Spacecraft Attitude Control Subsystem Hardware Critical Design Audit*. Northrop Grumman, 28 August 2013.
- [4] Hammann, Jeff. JWST Propellant Budget Document, Northrup Grumman. 19 July 2013. Document Number D40258
- [5] Gidanian, D., Wang, W., Fu, H. “ACS Thruster Firing Profile Analysis” PowerPoint Slides, 17 April 2013. 13-JWST-0135.
- [6] OPS TEM Session 3 – Mid Course Correction (MCC). Northrup Grumman Ground Operations/STScI, 31 January 2013.
- [7] Dipprey, N., “JWST Propulsion Burn Parameter Update: Based on Lasted Revised Propellant Budget Estimate of 12/12/2012”. PowerPoint Slides, 14 February 2013. 13-JWST-0136
- [8] McGregor, R., D., “JWST plume effects analysis summary: 2013 update”. PowerPoint Slides, 23 May 2013. 13-JWST-0186.
- [9] Grover, J., and Potter, G., “JWST Propulsion IDC”. Northrup Grumman. Redondo Beach, CA 90276, 14 March 2013. Mechanical Drawing, C327671 A.
- [10] “Injection Accuracy Post Launch Vehicle TIM”, Excel data from Arianespace through e-mail communication. November 2013.